Simulative Study on the Erosive Burning of Solid Rocket Motors

K. Yamada* and M. Goto†
National Defense Academy, Yokosuka, Japan

and

N. Ishikawa‡
University of California, Berkeley, Calif.

A simulative study is presented to clarify the characteristics of the flowfield in the grain port of a solid rocket motor under erosive burning conditions. The experiments are performed by using channels with porous walls and air flow at ambient temperature. It is shown that the boundary layer along the port develops rapidly similarly to pipe flow, which differs from Green's prediction. An empirical relation, similar to Lenoir-Robillard's semiempirical relation is obtained by correlating turbulence intensity with velocities and geometrical parameters of the channel. Thus, it is implied that an intimate relation exists between turbulence intensity and erosive burning.

Nomenclature

C_p = specific heat
D = inner diameter of a pipe (equivalent hydraulic diameter)
h = heat transfer coefficient
H = half height of two-dimensional channel
I = turbulence intensity
I_p = maximum value of turbulence intensity
k = constant
L = distance from the head end of a grain port
p = pressure
p_o = pressure at the head end of a grain port
p_L = pressure at $x=L$
q = heat flux
r = radial distance, surface regression rate or burning rate of a propellant
r_o = linear burning rate (without parallel flow)
r_e = burning rate increased caused by turbulence effect
R = radius of a pipe
R_e = Reynolds number; UD/ν
R_{eV} = Reynolds number; VD/ν
T = temperature
T_f = flame temperature
T_s = surface temperature
T' = fluctuating component of temperature
u = axial velocity component
u' = fluctuating component of u
U = maximum velocity of u at center line
U_t = threshold velocity
v = radial velocity component
v' = fluctuating component of v
V = transpiration flow velocity at surface
x = axial distance with origin at head end of a channel
y = distance perpendicular to surface with origin at wall
y' = distance perpendicular to surface with origin at center line
y_p = location of turbulence intensity at peak from the surface
β = constant
Δy = distance between flame front and surface
ϵ_e = thermal eddy diffusivity
η = $(r/R)^2$
κ = thermal diffusivity
λ = thermal conductivity
λ_e = equivalent thermal conductivity
ν = kinematic viscosity
ρ = density
Ψ = stream function

Presented as Paper 75-1201 at the AIAA/SAE 11th Propulsion Conference, Anaheim, Calif., Sept. 29-Oct. 1, 1975; submitted Oct. 9, 1975; revision received March 19, 1976. The authors are very grateful to K. Sumi and N. Kubota, at Technical Research and Development Institute of Japan Defense Agency, for their helpful discussions of this paper. They also wish to express their appreciation to M. Branch for his critical comments, and to J. Wirtanen for his correction of English, both at the University of California, Berkeley.

Index categories: Boundary Layers and Convective Heat Transfer-Turbulent, Solid and Hybrid Rocket Engines.

*Professor, Department of Aeronautical Engineering. Member AIAA.

†Assistant Professor, Department of Aeronautical Engineering.

‡Graduate Student, Department of Mechanical Engineering.

Introduction

A NUMBER of studies on the erosive burning of a solid propellant rocket motor have been conducted over the past thirty years.[1-3] Based on these studies, it has been concluded that erosive burning is attributed mainly to an increase in heat transfer from the hot gas flowing parallel to the burning surface. However, the characteristics of the flowfield in the grain port have not been clearly determined because of experimental difficulties in direct measurement in the motors due to high temperature, pressure and velocity of the gas, and time dependent regression of the burning surface. Therefore, the previous investigators could not compare their phenomenological arguments with experimental data characterizing the flowfield.

The direct measurement is performed here by means of a cold flow simulation in an attempt to obtain detailed information about the flowfield. One may expect to extract a law characterizing the flowfield which might be helpful to research into the flowfield in the rocket motors. It is meaningful to compare this result with the well-known properties of erosive burning obtained by using real rocket motors. This paper thus attempts to improve understanding of the mechanism of erosive burning by analysis of this comparison.

Lenoir and Robillard[4] presented a semiempirical relation for predicting the erosive burning rate in 1957. They assumed that the burning rate of a propellant under an erosive burning condition r is the sum of the two burning rates; one is the linear regression rate r_o obtained by the strand method, and the other is the burning rate increased due to the existence of the parallel flow to the burning surface. Thus they gave

$$r=r_o+k(U^{0.8}/L^{0.2})\exp(-\beta V/U) \quad (1)$$

This relation is also based on the assumption that the heat transfer to the burning surface is contributed to by two mechanisms; heat condition from the flame front with no parallel flow condition and turbulent heat convection from the "core flow" or central uniform flow. The Lenoir-Robillard relation is said to be in agreement with experimental results if one selects appropriate values for κ and β. Therefore, this relation will be used as a reference equation representing the result of the actual phenomenon to which to compare our results of simulation. It is, of course, necessary to take the limit of this analysis into account because the experimental conditions for both cases are different in terms of temperature, pressure, composition of gases, chemical reaction, and so on.

Apparatus and Procedure

Although an actual grain port has often a relatively complicated configuration, two simple geometries, circular and rectangular cross section, are used for the channel for experimental convenience. Most of the data are obtained with the rectangular channel, which consists of upper and lower walls with porous plates, 90 mm × 300 mm × 4 mm, having porosity 70μ or 20μ and side walls with transparent plastic plates. The distance between the two porous plates is selected to be 30 mm and 50 mm. As will be discussed later, the porous walls may have nonuniform porosity so that transpiration velocity cannot be expected to be uniform along the plates. The locations of the plates sometimes yield peculiar velocity distributions. To reduce this problem, an array of slits is used instead of the porous plates. The array consists of 2 mm slits and 2 mm copper slabs, which are arranged one by one. This is an extremely heterogeneous simulation which might be referred to as the solid propellant sandwich model studied by Nachbar.[5] Cylindrical channels with nonporous walls with various inside diameters (45, 52, 62, 100, and 126 mm) are also used for the comparison of the data with those of the porous channels. The measurements are performed at the location of 40 times the diameter downstream from the head end, where it is assured that the flow will be fully developed.

The air flow is supplied by a blower to the plenum chamber (Fig. 1), which is connected with the channel through the porous walls or slit arrays. The maximum velocity of axial flow available is about 40 m/sec at the center of the channel exit. Since it is necessary to have sufficient resistance to obtain relatively uniform flows through the walls, porous synthetic resin is attached to the slit array from the plenum sides. It is however, very difficult to get exactly uniform transpiration flow along the axial direction because of the static pressure drop due to the increase in mass flow rate along the channel.

Thus, air has been introduced only through the wall. Experiments are also performed by introducing the axial flow (called "main flow"), in addition to the transpiration flow, from the head end of the channel which is connected to a small wind tunnel with a separate blower. This is to simulate the experiments conducted by Marklund and Lake,[6] Zucrow,[7] Nadaud and Biasini.[8] They measured the erosive burning rate by placing a propellant segment in a test channel into which unburned gas generated by another motor was blown. To measure the axial velocity and turbulence intensity of the flowfield, a hot-wire anemometer made by Nihon Kagaku Kogyo is used, which is the constant temperature type. It indicates the time-averaged mean of the axial flow velocity, and root mean square value of turbulence intensity. For an I-type hot-wire probe, tungsten wire of 5μ diam is used, which is set perpendicular to the axial direction and parallel to the transpirating wall. The axial velocity in a circular channel is measured by means of a Pitot tube.

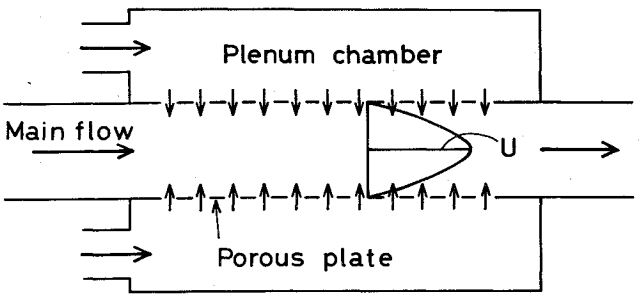

Fig. 1 Schematic of test channel.

Velocity Distribution

The axial velocity distribution indicates that the boundary layer develops rapidly, as shown in Fig. 2, for a rectangular channel with porous plates. Figure 3 shows the normalized curve as well as that of both laminar and turbulent flow in a pipe. It is observed that the curve for the porous channel shows a similar distribution pattern, but differs from the other two curves for a nonporous channel. Although a turbulent velocity distribution curve varies with the Reynolds number, the distribution with transpiration flow does not depend upon Reynolds number. Theoretical analysis (see Appendix) shows that the velocity distribution is independent of viscosity when the Reynolds number R_{eV} is sufficiently large. Thus, similar velocity distribution curves will be obtained for either laminar or turbulent flow.

The equations describing the velocity distribution are as follows, for a pipe with radius R:

$$u/U=\cos\{(\pi/2)\ (r/R)^2\} \quad (2)$$

$$v/V=-(R/r)\sin\{(\pi/2)\ (r/R)^2\} \quad (3)$$

and for a two-dimensional channel with height $2H$:

$$u/U=\cos\{(\pi/2)\ (y'/H)\} \quad (4)$$

$$v/V=-\sin\{(\pi/2)\ )y'/H)\} \quad (5)$$

Figure 3 shows the theory to be in good agreement with experimental data.

Green[9] presumed that the axial velocity in the core flow, which is outside of the boundary layer, is uniform, and the boundary-layer thickness decreases as axial velocity increases. He was thus led to infer that erosive burning might be caused by a decrease in the boundary-layer thickness. This concept has been adopted by many investigators. However, according to Fig. 2, it can be seen that the boundary layer develops rapidly because of mass addition from the wall. It is conceivable that the boundary layer in an actual grain port also develops rapidly since there may not be much difference in mass and momentum transport mechanisms. In addition, the transpiration flow velocity might be about the same order of magnitude as that of this simulative experiment. Although there are differences between both cases in some other factors such as temperature, pressure, composition of gases, chemical reaction and so forth, these influences to the velocity distribution would be of secondary importance compared to the fluid dynamical factors. For the fully developed flow, the Lenoir-Robillard relation should be corrected by replacing the distance L by a pipe diameter D. This modified form will be adopted in the following portion of this paper.

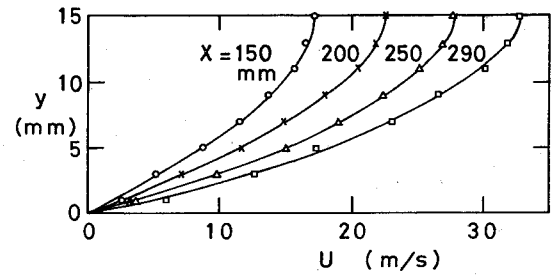

Fig. 2 Axial velocity distribution at various locations ($2H = 30$ mm, porosity $= 20\mu$).

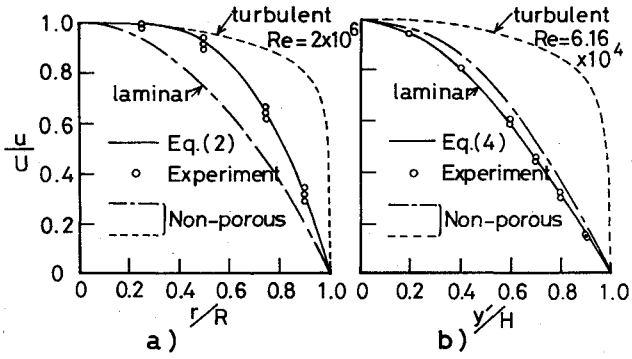

Fig. 3 Normalized velocity distribution: a) pipe flow; b) two-dimensional flow.

In explaining erosive effect, thus, it is not adequate to attribute it to the variation of boundary-layer thickness as in the case with no chemical reaction, because in this reactive case the temperature of gases varies mainly within the region between the flame front and the surface. When the flow has a similar velocity distribution, the transverse velocity v is proportional to the transpiration velocity V as in the Eq. (3) and the Eq. (5). Then, providing that every particle that leaves the burning surface reacts after a constant time lag, the flame height must increase as V increases or as the axial distance increases. Hence, Green's concept on erosive burning seems to fail because of the wrong presumption of the flowfield.

It would be more consistent to view the mechanism of erosive burning in terms of turbulent motion of the gases. The role of turbulence adjacent to the wall is not only to increase the heat transfer, but also to enhance the mixing rate of decomposition gases so that ignition time lag will effectively be reduced. Similar concepts have already been suggested by many other investigators such as Corner[10] and Vandenkerckhove;[11] however, it should be noticed that none of them showed experimental evidence for the properties of the flowfield. It is now desirable to obtain quantitative characteristics of the turbulence near the wall. This will be discussed in the next sections.

Turbulence Intensity Distribution

The turbulence intensity distribution curves measured at several locations of a rectangular channel over half-cross-section is shown in Fig. 4, which shows a similar trend to those for a nonporous tube shown earlier by Laufer[12] and others. In Fig. 4, dimensional values of turbulence intensity are plotted because we are concerned with the magnitude of turbulence intensity rather than normalized values. This is because it will be a rather pertinent factor in discussing the increase in heat transfer with turbulence. A number of small, irregular waves are observed near the wall. This is supposed to be due to nonhomogeneous porosity of the porous plate because of their reproduceability. It is seen in Fig. 4 that the magnitude of the maximum value of turbulence intensity at the peak I_p increases,and the distance between the peak and

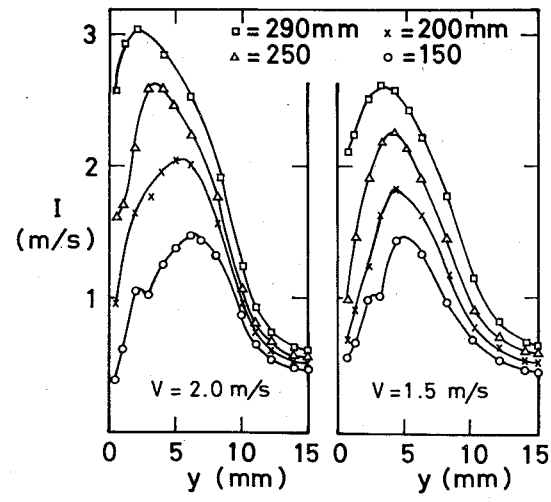

Fig. 4 Turbulence intensity distribution ($2H = 30$ mm, porosity $= 70\mu$).

the wall y_p decreases as the axial velocity increases. Since I_p and y_p change at the same time with respect to the axial velocity U "turbulence gradient," which is defined by I_p/y_p, will be a reasonable factor in order to characterize the behavior of turbulence near the wall. In practice, with some condition of velocities, y_p becomes too small to be measured by a hot-wire anemometer.

Turbulence Intensity at Peak I_p

The relation between turbulence intensity and the axial velocity for various cases is shown in Figs. 5–8. It is seen that the data lie as a whole on a straight line with gradient 0.8. Hence, I_p seems to be proportional to $U^{0.8}$. It is quite interesting to see that I_p is a function only of U and independent of the axial location and V. In other words, the magnitude of turbulence near the wall is almost independent of the past history of flow and the transpiration velocity. On the range of small U, the data show a different aspect. Under these conditions it is observed that the velocity fluctuates with low frequency. An irregular distribution of turbulence is observed very near the wall for both cases of porous plate and slit wall. This is due to the nonuniform porosity of a porous wall and the discontinuity of a slit wall. Then, Figs. 5 and 6 imply that such a heterogeneity of a wall will be a secondary factor for turbulence generation compared to the effect of the axial velocity U.

The decrease in I_p in the region of small U in Fig. 7 may be considered to be in a transition region from laminar to turbulent flow. It should be noticed that the abscissa in Fig. 8 is $U^{0.8}/D^{0.2}$ to take the scale effect into account. Although the velocity distribution changes slightly with respect to Reynolds number, its influence on the relation $I_p \propto U^{0.8}$ seems negligible. Thus, the $I_p \propto U^{0.8}$ is one of the laws of the flowfield near the wall that we hoped to extract. The interesting point about this law is that it holds independently of the wall condition and of the velocity distribution.

Behavior of y_p

Figures 9 and 10 show how y_p changes with respect to the transpiration velocity and the main flow velocity. Figure 9 indicates y_p is proportional to the factors $\exp(\beta' V)$, Fig. 10 shows the relation $y_p \propto \exp(\beta''/U)$, and Fig. 11 implies that these relations will be combined to yield

$$y_p \propto \exp(\beta V/U) \tag{6}$$

The large deviation of the data, as in upper right corner of Fig. 11, corresponds to the region of small U. The relation (6) may not hold in this region.

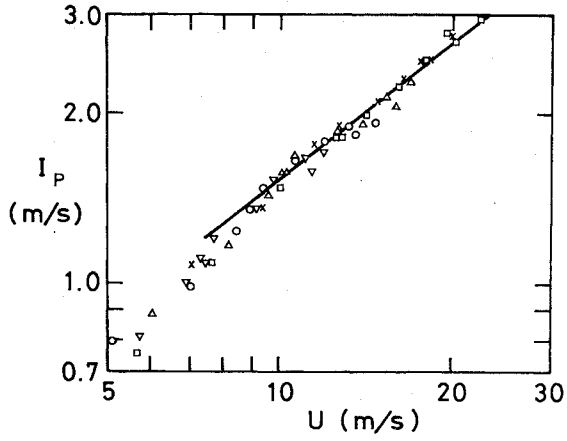

Fig. 5 Correlation between maximum turbulence intensity I_p and maximum flow velocity U for porous wall with porosity 20μ without main flow.

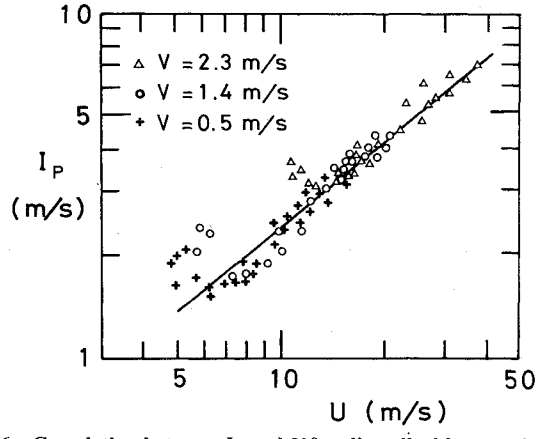

Fig. 6 Correlation between I_p and U for slit wall without main flow.

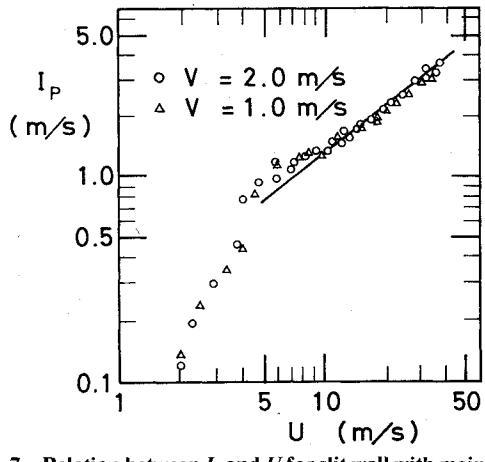

Fig. 7 Relation between I_p and U for slit wall with main flow.

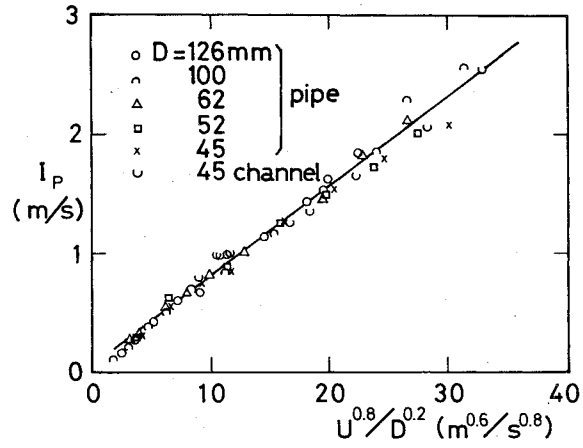

Fig. 8 Relation between I_p and factor $U^{0.8}/D^{0.2}$ nonporous pipe flow.

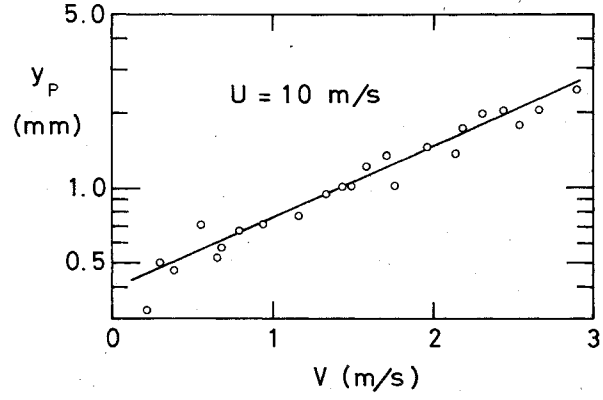

Fig. 9 Relation between peak distance y_p and blowing velocity V with constant main flow velocity.

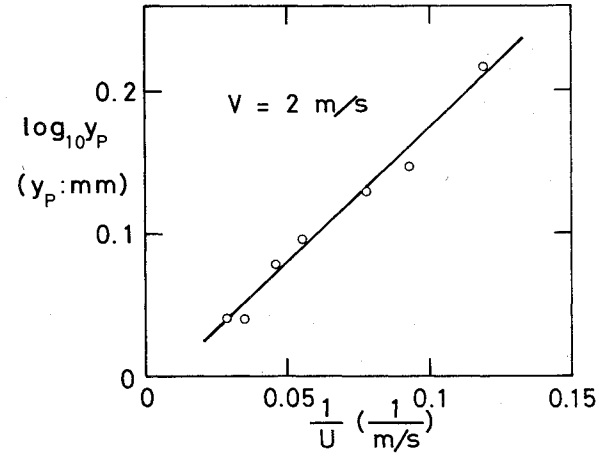

Fig. 10 Relation between peak distance v_p and reciprocal of main flow velocity U with constant blowing velocity.

Characteristic of Turbulence and Heat Transfer

We are now in a position to examine the results in comparison with the law of heat transfer and erosive burning. From the results in the previous section, we may obtain the turbulence gradient as

$$I_p/y_p \propto (U^{0.8}/D^{0.2})\exp(-\beta V/U) \tag{7}$$

The right-hand side of this equation is exactly the same form as the heat transfer equation for a circular tube flow with $Pr \simeq 1$, i.e.

$$hD/\lambda \propto (UD/\nu)^{0.8}\exp(-\beta V/U) \tag{8}$$

It is remarkable that it also has the same form as the second term (erosion term) of the Lenoir-Robillard equation. This implies that there must be an intimate relation between the erosion effect and the turbulence gradient. In order to explicitly view the relationship between the turbulence intensity and heat transfer, an auxiliary experiment is performed by using a sublimative sample of paradichlorobenzene (21.7 mm

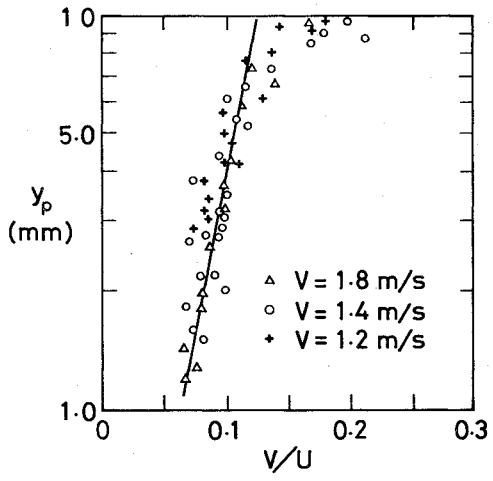

Fig. 11 Relation between velocity ratio V/U and distance y_p, for slit wall without main flow.

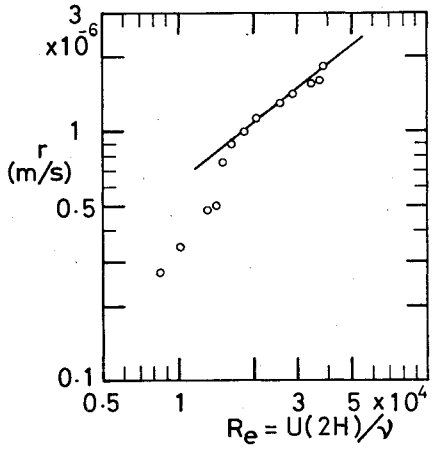

Fig. 12 Correlation between surface regression rate of sublimating material and Reynolds number with hot main flow.

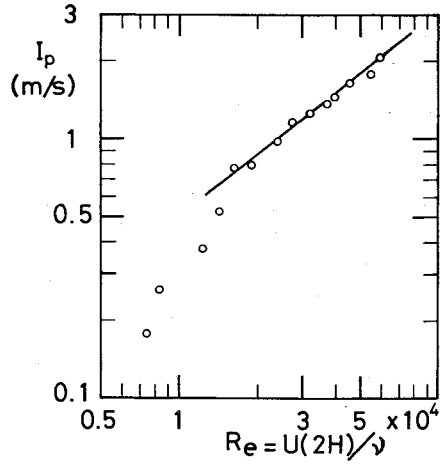

Fig. 13 Correlation between y_p and Reynolds number for the same channel as Fig. 12 without transpiration.

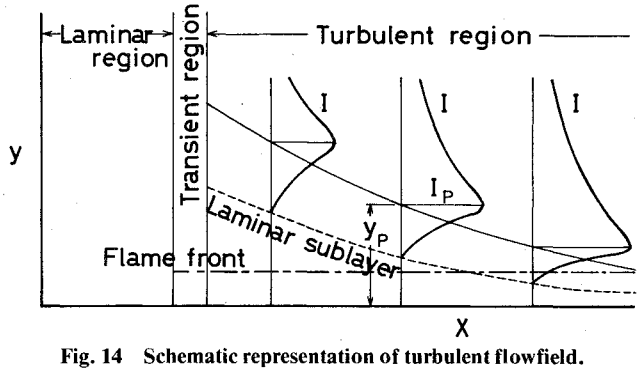

Fig. 14 Schematic representation of turbulent flowfield.

diam., 6 mm thick). This specimen is placed in a rectangular channel (30 mm×90 mm) with nonporous wall, through which hot air at 50° C±1° C, is introduced. The regression rate r and turbulence intensity are measured with respect to Reynolds number; the results are shown in Figs. 12 and 13. Both of the figures show remarkable similarity. It should be noted that the similarity holds not only in the region of 0.8 power law, but also in the transition region. It can then be inferred that there must be a proportional correlation between heat transfer and turbulence intensity.

Turbulence and Erosive Burning

According to Summerfield[13] and others, the combustion reaction takes place in the vicinity of the burning surface, typically within 100μ. If we assume a linear temperature profile, the heat transfer from the flame to the surface is given by

$$q=\lambda_e(T_f-T_s)/\Delta y \tag{9}$$

We also have

$$q=-\lambda \mathrm{d}T/\mathrm{d}y+\rho C_p<v'T'> \tag{10}$$

where the first term of the right-hand side is heat flux caused by molecular conduction, and the second is additional heat flux due to turbulent mixing. If we use the turbulent thermal diffusivity ϵ_e, Eq. (10) is written in the form

$$q=-\rho C_p(\kappa+\epsilon_e)\mathrm{d}T/\mathrm{d}y \tag{11}$$

Then, the equivalent thermal conductivity becomes $\lambda_e=\rho C_p(\kappa+\epsilon_e)$. If the burning rate r is proportional to heat flux q, we may get

$$r=r_o+r_e \tag{12}$$

where r_o denotes the burning rate caused by molecular conduction and r_e denotes the burning rate increased due to turbulence effect. On the other hand, Lenoir and Robillard interpreted r in Eq. (12) as the sum of the burning rate due to conduction under the strand burning condition and the burning rate due to convective heat flux from the core flow. Strictly speaking, their interpretation of Eq. (12) is not correct because the temperature distribution under the convective condition is different from that of the strand burning condition. In fact, r_o and r_e must be subject to the same temperature distribution. However, the temperature distribution depends actually upon factors such as turbulence intensity, ignition time lag, properties of burned gases, and so forth. So, for convenience, Eq. (12) may be adopted if we use an appropriate constant in the r_e term. This is constant k in Lenoir-Robillard relation and k accounts for all the tedious problems that turbulence effects cause.

Marlund-Lake's experiment shows that the effect of composition and mixture ratio of the propellant become small as pressure increases.[6,14] This phenomenon could be explained as follows. It has been known that at high pressure, the deflagration of Ammonium Perchlorate AP is predominant so that AP particles recess faster than the binder. When there exists a strong parallel flow, the heat transfer from the flame to the convex binder increases and consequently the propellant surface will become flatter. Then the influence of the properties of the binder becomes small.

Threshold Phenomenon

The interpretation of the threshold phenomenon has been one of the most difficult problems of study for erosive burning. The threshold phenomenon is observed in experiments in the laboratory as well as in an actual rocket motor. The threshold velocity varies with respect to the properties of a propellant and pressure. Then, it cannot be satisfactorily explained by either the conditions near the head end of a motor or transition of the flow from laminar to turbulent boundary layer. There exists, of course, a laminar sublayer in the turbulent region the thickness of which is expected to decrease toward the exit. Figure 14 shows the relative position between the boundary of the laminar region and the flame front. As assumed by Vandenkerckhove,[11] the threshold velocity U_t corresponds to the velocity at which the boundary curve of the laminar sublayer crosses the flame front line. It has been known that the larger the strand burning rate r_o, the larger is the threshold velocity u_t. This can be explained by shifting the flame front line closer to $y=0$ or the boundary of laminar sublayer further away from $y=0$ due to larger blowing for a higher burning rate propellant and, accordingly, the corresponding intersection moves to a larger x coordinate or equivalently larger U_t. This model also enables us to understand the fact that the erosive burning rate is smaller for a propellant with larger r_o. That is, turbulence influence will become less effective, since the intersection of the higher burning rate propellant moves to a larger axial coordinate of the grain port than that of the lower burning rate propellant.

Negative erosion has not been clarified yet. The authors attempted to interpret this phenomenon in terms of weak turbulent motion of the flow near the head end of the port. According to the experiment for oscillatory combustion with the two-motors method conducted by Crump and Price,[15] strong oscillation increases the burning rate, while weak oscillation retards it. Since turbulence is a kind of irregular oscillation, it is conceivable that weak turbulent motion of the flow could be a cause of negative erosion. In other words, such weak turbulence as may exit in the laminar region influences the flame front and, as a result, retards the combustion.

Summary

A simulative study is presented to clarify some of the unresolved problems on the erosive burning of a solid propellant rocket motor. The experiments are performed by using channels with porous walls, through which air at ambient temperature is transpirated. As a result, the following is clarified or presumed. The boundary layer develops rapidly in a transpirating channel and the velocity distribution indicates a unique similarity, which differs from Green's prediction. In the turbulent region, the maximum value of turbulence intensity near the wall I_p is proportional to the 0.8 power of axial velocity. This relation is independent of the value of both transpiration and axial location. For the fully developed flow in the pipe without transpirating flow, I_p is also proportional to 0.8 power of U although the velocity distribution is different from that in a transpirating channel. For small U, laminar and transition regions exist, weak turbulence with low frequency is observed. However, the flow does not obey the 0.8 power law in these regions. There exists an intimate relation between turbulence intensity and rate of heat transfer and consequently between turbulence intensity and erosive burning rate.

Appendix: Derivation of Similar Solution

The flow will be treated as viscous laminar flow. For the axisymmetrical pipe flow of incompressible fluid, the equations of motion and continuity equation are described as follows:

$$u\frac{\partial u}{\partial x}+v\frac{\partial u}{\partial r}=-\frac{1}{\rho}\frac{\partial p}{\partial x}+\nu\left\{\frac{1}{r}\frac{\partial}{\partial r}\left(r\frac{\partial u}{\partial r}\right)+\frac{\partial^2 u}{\partial x^2}\right\} \quad \text{(A1)}$$

$$u\frac{\partial v}{\partial x}+v\frac{\partial v}{\partial r}=-\frac{1}{\rho}\frac{\partial p}{\partial r}+\nu\left[\frac{\partial}{\partial r}\left\{\frac{1}{r}\frac{\partial}{\partial r}(rv)\right\}+\frac{\partial^2 v}{\partial x^2}\right] \quad \text{(A2)}$$

$$\frac{\partial(ru)}{\partial x}+\frac{\partial(rv)}{\partial r}=0 \quad \text{(A3)}$$

The boundary conditions are

$$\text{at center } r=0;\ v=0,\ \partial u/\partial r=0 \quad \text{(A4)}$$

$$\text{at wall } r=R;\ v=-V,\ u=0 \quad \text{(A5)}$$

Introducing the stream function Ψ, we obtain

$$ru=\partial\Psi/\partial r, \qquad rv=-\partial\Psi/\partial x \quad \text{(A6)}$$

and the following form is assumed for similar solution:

$$\Psi(x,r)=Rf(r)\int_0^x V\mathrm{d}x \quad \text{(A7)}$$

hence

$$u=\{Rf'(r)/r\}\int_0^x V\mathrm{d}x \quad \text{(A8)}$$

$$v=-VRf(r)/r \quad \text{(A9)}$$

Substituting Eqs. (A8) and (A9) into (A1)

$$\frac{VR}{\nu}\left\{\left(\frac{f'}{r}\right)^2-\frac{f}{r}\left(\frac{f'}{r}\right)'\right\}-\frac{1}{r}\left\{\left(\frac{f'}{r}\right)'+r\left(\frac{f'}{r}\right)''\right\}=-\left(\frac{\mathrm{d}p}{\mathrm{d}x}\right)\Big/\{\mu R\int_0^x V\mathrm{d}x\} \quad \text{(A10)}$$

If VR/ν is sufficiently large everywhere, the second term of the left-hand side becomes negligible. Then, substituting $\eta=(r/R)^2$, Eq. (A10) becomes

$$(\mathrm{d}f/\mathrm{d}\eta)^2-f(\mathrm{d}^2f/\mathrm{d}\eta^2)=-R^2(\mathrm{d}p/\mathrm{d}x)/4\rho V\int_0^x V\mathrm{d}x) \quad \text{(A11)}$$

As the left-hand side is a function of η only and the right-hand side is a function of x only, the equality is obtained only when both are constant.

It is shown simply that the expression $f=\sin(\pi\eta(2)$ satisfies the previous equation and boundary conditions. Thus

$$u/U=\cos(\pi\eta/2) \quad \text{(A12)}$$

$$v/V=-(R/r)\sin(\pi\eta/2) \quad \text{(A13)}$$

Where

$$U=(\pi/R)\int_0^x V\mathrm{d}x \quad \text{(A14)}$$

That is, the center velocity U increases with x, and the velocity distribution u increases also with U, but u/U has a definite similar distribution independent of x. Furthermore, radial velocity distribution v/V has the same form everywhere. From the right-hand side of Eq. (A11)

$$\mathrm{d}p/\mathrm{d}x=-(\pi^2\rho V/R^2)\int_0^x V\mathrm{d}x \quad \text{(A15)}$$

Especially, if $V=$ const, the pressure drop is

$$(p_o-p)\ /\ (p_o-p_L)=(x/L)^2 \quad \text{(A16)}$$

In order to obtain the condition that the second term of left-hand side in Eq. (A10) is smaller than 1% of first term, calculation was done by substituting $f=\sin(\pi\eta/2)$, resulting in $VR/\nu<514$. Using the values of certain test, for instance,

$R=0.02$ m, $\upsilon=1.56\times10^{-5}$ m^2/sec (20° C, 1 atm), $V<0.40$ m/sec is obtained, which can give an approximate range for similar distribution. For a two-dimensional channel flow, almost the same treatment can show the existence of similar distribution.

References

[1]Williams, F. A., Barrère, M., and Huang, N. C., *Fundamental Aspects of Solid Propellant Rockets*, AGARDograph 116, 1969, Chap. 7, pp. 395-456.

[2]Murphy, J. M., "A Summary of the Results of Experimental Investigations of Erosive Burning," *Third Conference on the Performance of High Temperature Systems*, Pasadena, Calif., Dec. 1964, pp. 247-258.

[3]Murphy, J. M., "Analytical Approaches to Erosive Burning," *Third Conference of Performance of High Temperature Systems*, Pasadena, Calif., Dec. 1964, pp. 259-270.

[4]Lenoir, J. M. and Robillard, G., "A Mathematical Method to Predict the Effects of Erosive Burning in Solid Propellant Rockets," *Sixth Symposium (International) on Combustion*, Reinhold, New York, 1957, pp. 663-667.

[5]Nachbar, W., and Parks, J. M., "A Sandwich Burner Model for the Composite Solid Propellant," Lockheed Missile System Division 2191, AFOSR-RN57-418, AD132-497, 1957.

[6]Marklund, T. and Lake A., "Experimental Investigation of Propellant Erosion," *ARS Journal*, Vol. 30, Feb. 1960, pp. 173-178.

[7]Zucrow, M. J., Osborn, J. R., and Murphy, J. M., "An Experimental Investigation of the Erosive Burning Characteristics of a Non-Homogeneous Solid Propellant," AIAA Paper 64-107, 1964.

[8]Nadaud, L. and Biasini, J., "Ablation de Combustibles Solides Utilises dans les Fusees Hybrides," *La Recherche Aerospatiale*, No. 115, Nov.-Dec. 1966, pp. 45-55.

[9]Green, L., "Erosive Burning of Some Composite Solid Propellants," *Jet Propulsion*, Vol. 24, Jan.-Feb. 1954, pp. 9-15.

[10]Corner, J., "The Effect of Turbulence on Heterogeneous Reaction Rates," *Transactions of the Faraday Society*, Vol. 43, 1947, pp. 635-642.

[11]Vandenkerckhove, J. A., "Erosive Burning of a Colloidal Solid Propellant," *Jet Propulsion*, Vol. 28, Sept. 1958, pp. 599-603.

[12]Laufer, J., "Investigation of Turbulent Flow in a Two-Dimensional Channel," NACA TR-1053, 1950, pp. 1247-1266.

[13]Summerfield, M., Sutherland, G. S., Webb, M. J., Taback, H. J., and Hall, K. P., "Burning Mechanism of Ammonium Perchlorate Propellants," *Progress in Astronautics and Rocketry*, Vol. 1, Academic Press, New York, 1960, pp. 141-182.

[14]Vandenkerckhove, J. and Jaumotte, A., "Remarks on the Burning Mechanism and Erosive Burning of Ammonium Perchlorate Propellants," *Eighth Symposium (International) on Combustion*, Williams & Wilkins, Baltimore, Md. 1962, pp. 689-693.

[15]Crump, J. E., and Price, E. W., "Effect of Acoustic Environment on the Burning Rate of Solid Propellants," *AIAA Journal*, Vol. 2, July 1964, pp. 1274-1278.